Title
Modeled foraminiferal calcification and strontium partitioning in benthic foraminifera helps reconstruct calcifying fluid composition

Journal
Communications Earth & Environment, 5(1)

ISSN
2662-4435

Authors
Jia, Qicui
Zhang, Shuo
Watkins, James M
et al.

Publication Date
2024-01-12

DOI
10.1038/s43247-023-01194-6

Peer reviewed

communications
earth & environment

ARTICLE

https://doi.org/10.1038/s43247-023-01194-6 OPEN

Modeled foraminiferal calcification and strontium partitioning in benthic foraminifera helps reconstruct calcifying fluid composition

Qicui Jia[1], Shuo Zhang[1]✉, James M. Watkins[2], Laurent S. Devriendt[3], Yuefei Huang[1,4] & Guangqian Wang[1]

Foraminifera are unicellular organisms that inhabit the oceans. They play an important role in the global carbon cycle and record valuable paleoclimate information through the uptake of trace elements such as strontium into their calcitic shells. Understanding how foraminifera control their internal fluid composition to make calcite is important for predicting their response to ocean acidification and for reliably interpreting the chemical and isotopic compositions of their shells. Here, we model foraminiferal calcification and strontium partitioning in the benthic foraminifera *Cibicides wuellerstorfi* and *Cibicidoides mundulus* based on insights from inorganic calcite experiments. The numerical model reconciles inter-ocean and taxonomic differences in benthic foraminifer strontium partitioning relationships and enables us to reconstruct the composition of the calcifying fluid. We find that strontium partitioning and mineral growth rates of foraminiferal calcite are not strongly affected by changes in external seawater pH (within 7.8–8.1) and dissolved inorganic carbon (DIC, within 2100–2300 μmol/kg) due to a regulated calcite saturation state at the site of shell formation.

[1] State Key Laboratory of Hydroscience and Engineering, Department of Hydraulic Engineering, Tsinghua University, Beijing, China. [2] Department of Earth Sciences, University of Oregon, Eugene, OR 97403, USA. [3] Chemical Sciences Division, Lawrence Berkeley National Laboratory, Berkeley, CA 94720, USA. [4] State Key Laboratory of Plateau Ecology and Agriculture, Qinghai University, Xining, Qinghai 810016, China. ✉email: zhangs2019@tsinghua.edu.cn

Trace element uptake by calcite ($CaCO_3$) during mineral growth is sensitive to environmental parameters such as solution composition, temperature and pH. This is the basis for using trace elements to infer the conditions of carbonate mineral formation, with the caveat that trace element concentrations often record a convolution of multiple environmental variables. For example, the partitioning of strontium (Sr) into inorganic calcite (partition coefficient $D_{Sr} = [Sr/Ca]_{calcite}/[Sr/Ca]_{fluid}$), has long been known to be dependent on both temperature (T) and growth rate (R_p)[1–6]. A reassessment of previous studies has revealed that the D_{Sr}-R_p relationship for inorganic calcite varies systematically with solution pH, and an ion-by-ion model for crystal growth has been developed to account for this effect[7,8]. These developments present an opportunity to revisit comparisons in Sr partitioning behavior between inorganic calcite and other calcites produced through biologically-mediated processes.

Foraminifera are unicellular organisms that inhabit the oceans and make calcite tests (shells). As with inorganic calcite, much effort has been devoted to understanding the controls on D_{Sr} of foraminiferal calcite through culturing experiments of benthic (ocean floor and sediments) and planktonic (surface oceans) foraminifera[9–18]. One of the main conclusions from these studies is that trace element discrimination is unique to each species, due to distinct evolutionary adaptation strategies in the biological shell-building process. Among these adaptations is the ability to modify seawater chemistry in a small volume near the site of calcification that is difficult to probe directly. A longstanding question is to what extent geochemical differences between different calcifying species and inorganic calcite (e.g., refs. [19–21]) can be explained by the (unknown) modified seawater composition as opposed to additional biological effects (e.g., influences from organic molecules[22]).

Here, we assess whether D_{Sr} values in foraminifera can be explained by inorganic-like partitioning within a biologically-modified calcifying fluid. Previous work has identified key processes by which foraminifera control their internal fluid composition, such as seawater intake through vacuoles[23], proton pumping to increase pH[24], and transmembrane ion transport[25–27]. These processes are included in a model for coral calcification[28], and here we adopt this existing framework but with a key modification: the Sr/Ca of calcite is calculated from the modeled calcifying fluid composition ($[DIC]_{cf}$, pH_{cf}, $[Ca^{2+}]_{cf}$, $[Sr^{2+}]_{cf}$) using the aforementioned ion-by-ion model that was calibrated against Sr/Ca data from inorganic calcite[8].

Previous studies have reported Sr/Ca ratios from cultured foraminifera[9–18], natural planktonic foraminifera[29–34] and benthic foraminifera[35–44]. Here, we focus our analysis to core-top data from modern benthic foraminifera for several reasons: (1) the temperature at depth is more constant than in the surface waters where planktonic species thrive, (2) the depth at which benthic foraminifera are collected can be assumed to represent the depth at which they formed, (3) the seawater saturation state ($\Omega_{sw} = [Ca^{2+}]_{sw}[CO_3^{2-}]_{sw}/K_{sp}$) of calcite has been reported or can be estimated from the GLODAP database[45], (4) individual species of benthic foraminifera have been collected from all ocean basins at a wide range of water depths (1 to 5 km), leading to a dataset that spans a wide range in D_{Sr}, and (5) the selected foraminiferal species have low Mg/Ca (<20 mmol/mol), which makes it applicable to our low-Mg calcite model of Sr partitioning (i.e., high Mg is known to affect Sr incorporation into calcite[7,46]).

The core-top data from Yu et al.[36] reveal a strong relationship between D_{Sr} and seawater calcite saturation state (Ω_{sw}) for the benthic species *Cibicidoides wuellerstorfi* (*C. wuellerstorfi*) and *Cibicidoides mundulus* (*C. mundulus*, Fig. 1). It is clear, however,

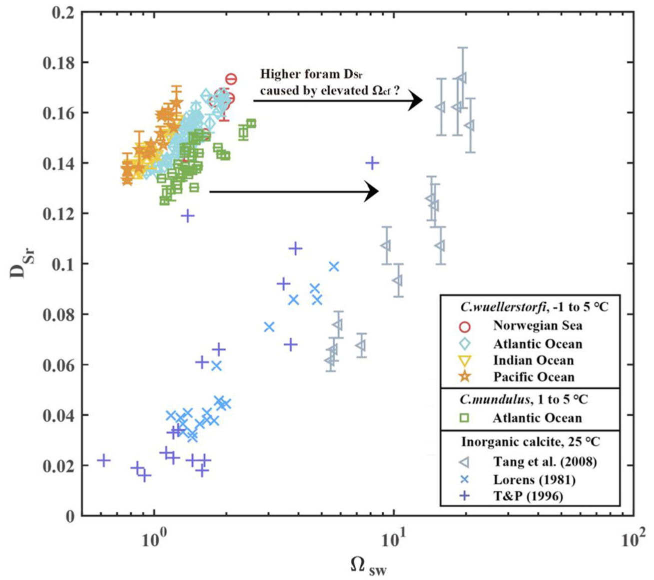

Fig. 1 The Sr partition coefficient between calcite and solution (D_{Sr}) for foraminifers and inorganic calcite as a function of the environmental calcite saturation state (Ω_{SW}). The foraminifera samples[36] come from *C. wuellerstorfi* in the Norwegian Sea (red circle), the Atlantic Ocean (blue rhombus), the Indian Ocean (yellow triangle) and the Pacific Ocean (orange star), and *C.mundulus* in the Atlantic Ocean (green square). The offset in Sr partition coefficient (D_{Sr}) between foraminiferal and inorganic calcite[1–3] (gray triangle, blue cross and purple cross) may be caused by elevated calcite saturation state (Ω) at the site of calcification in the foraminifera. Errors in foraminiferal D_{Sr} data[36] represent ±1σ of replicates. Errors in inorganic data[3] are $\pm 0.07 * D_{Sr}$.

that Ω_{sw} is not the primary variable controlling foraminiferal D_{Sr}, as there are offsets in the D_{Sr}-Ω_{sw} relationships among *C. wuellerstorfi* samples collected from different ocean basins as well as an offset between *C. wuellerstorfi* and *C. mundulus* for specimens that calcified at the same locations. These variable foraminiferal D_{Sr}-Ω_{sw} relationships lack a clear explanation. The partitioning of Sr between inorganic calcite and solution displays similar D_{Sr} sensitivities to Ω_{sw} but with lower D_{Sr} values at a given Ω_{sw}. The magnitude of the offset in D_{Sr} between foraminiferal and inorganic calcite is consistent with a 10-fold increase in Ω at the site of calcification (Ω_{cf}) in the foraminifera (Fig. 1). Here, we test if known biocalcification mechanisms can explain the offset in D_{Sr}-Ω_{sw} relationships: (1) between foraminiferal and inorganic calcite, (2) between foraminifers from different ocean basins, and (3) between foraminiferal taxa. We show that our model can explain inter-ocean and taxonomic differences in benthic D_{Sr} relationships and provides constraints on the foraminiferal calcifying fluid composition.

In addition, D_{Sr} data from culturing experiments conducted under a wider range of seawater chemistry conditions are used to assess the limits of our model assumptions and applications to both benthic and planktonic foraminifera[9,17,18]. In particular, we evaluate the required rates of alkalinity pumping rate in our model to match experimentally measured D_{Sr} values under varying pH and DIC conditions. Results from culture experiments suggest that each foraminifera species has a distinct alkalinity pumping rate, but this parameter remains relatively constant under varying seawater pH. Finally, assuming time-independent model parameters, we apply our model to infer past and future changes in foraminiferal calcifying fluid composition, calcite growth rate and Sr partitioning based on historical and projected atmospheric CO_2 concentrations.

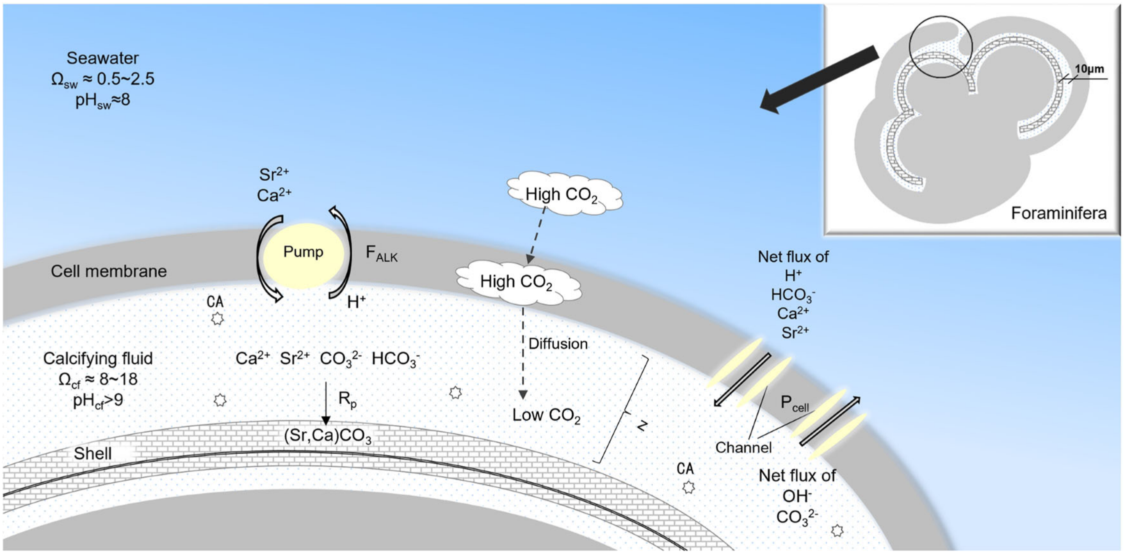

Fig. 2 Schematic diagram of foraminiferal calcification. The site of calcification is conceptualized as a box with unit surface area and a height of z. Active proton pumping (F_{ALK}), CO_2 diffusion, transmembrane transport of ions (characterized by the cell permeability P_{cell}), calcite precipitation (R_p), and carbonic anhydrase (CA) are considered in this model.

Results and discussion

Processes involved in foraminiferal calcification. Foraminifers precipitate their shells from modified seawater within a closed or semi-closed environment[25]. Previously identified biomineralization processes relevant to calcite growth kinetics and trace element partitioning include: (1) transfer of seawater to the calcifying space through passive leakage or active vacuolization, or transmembrane transport of ions (through pumps or channels) to the site of calcification[25,47], (2) a diffusive flux of $CO_{2(g)}$ from the high [CO_2] cellular space[20] and/or environmental seawater[48] towards the calcifying fluid, (3) active H^+ removal from the calcifying fluid coupled with cation pumping to the calcifying space for charge balance (e.g., Ca^{2+}[24,48]), and (4) the presence of the enzyme carbonic anhydrase, which rapidly converts $CO_{2(aq)}$ into HCO_3^- in the calcifying fluid[49]. Processes 1 and 2 act to transport DIC from seawater[25]. A comparison of foraminiferal D_{Sr} values[36] with the environmental concentrations of individual DIC species (see Supplementary Notes 1) suggests environmental DIC and/or HCO_3^- (process 1) is/are the main source(s) of carbon for calcite precipitation in these taxa while environmental or metabolic $CO_{2(aq)}$ (process 2) is not, consistent with previous observations in decoupled carbonate-system experiments[14,18] and biomineralization models based on oxygen isotope data[50,51].

The above processes are accounted for in the model with some simplifications:

1. We cast the flux of ions from seawater or seawater vacuoles to the calcifying fluid as being proportional to the concentration gradient through a membrane permeability coefficient (m s^{-1}):

$$P_{\text{cell}} = \frac{k \cdot D}{\Delta x} \tag{1}$$

where k is a dimensionless quantity that characterizes the interaction between the ion and membrane, D is a diffusion coefficient (m^2 s^{-1}), and Δx is membrane thickness (m). We treat P_{cell} as being the same for all ions that we track (i.e., Ca^{2+}, Sr^{2+}, HCO_3^-, CO_3^{2-}, H^+, and OH^-) as membrane ionic affinities remain unknown. Although our model does not include Mg, we note that P_{cell} would need to be much smaller for Mg^{2+} in order to explain the extremely low Mg/Ca (2-6 mmol/mol at 5 °C[47]) relative to seawater Mg/Ca (5200 mmol/mol). Our treatment of the ion flux does not distinguish explicitly between seawater vacuolization and transmembrane transport of ions because we use the same values of P_{cell} for HCO_3^- and CO_3^{2-}. The mathematical representation of HCO_3^- and CO_3^{2-} through transmembrane transport (terms with P_{cell} in Eq. 2) is equivalent to that for direct uptake of seawater DIC and alkalinity (terms with τ_{sw} in Eq. 2) insofar as the ion flux is proportional to the concentration difference between seawater and the calcifying fluid. Analysis of the Mg content of foraminiferal calcite (see Supplementary Notes 2) suggests that transmembrane transport is the dominant process through which foraminifera gains ions for calcification in low-Mg foraminifera. We, therefore, set the vacuolization terms to zero and only include transmembrane transport. Toyofuku et al.[48] shows that seawater pH is lower in a boundary layer surrounding foraminifera due to pumping of H^+, and therefore, a fraction of the DIC may enter the site of calcification via CO_2 diffusion from this layer. Similarly to their model[48], the uptake of DIC for calcification in our model is strongly dependent on the concentration gradient between seawater and the calcifying fluid, although we do not address explicitly differences in the proportions of DIC species between seawater and a boundary layer.

2. The high [CO_2] cellular space is assumed to have a concentration of 13 μmol/kg, as was assumed for a coral calcification model[28]. This is a similar value as seawater [CO_2] at pH = 8.2 and T = 5 °C. Hence, our model does not distinguish between CO_2 from the cellular space versus that from seawater.

3. A cation alkalinity pump increases the pH of the calcifying fluid by exchanging two H^+ for one Ca^{2+} or Sr^{2+}[24,48]. The proportions of exchanged Ca^{2+} and Sr^{2+} are assumed to follow their ratios in seawater, i.e., there is no Sr/Ca fractionation during pumping. If other cations were to be involved in exchanging for H^+, then the Sr^{2+} and Ca^{2+} fractions of the alkalinity pump (*f*) could be decreased accordingly.

4. We treat the DIC species as being instantaneously equilibrated, implying that the concentration of carbonic anhydrase is sufficient for the DIC equilibration time to be much shorter than the residence time of DIC in the calcifying fluid[52].

A schematic of the model is presented in Fig. 2. Mathematically, the model involves four coupled ordinary differential equations (ODEs) that track the concentrations of Ca^{2+}, Sr^{2+}, alkalinity, and DIC in the calcifying fluid as they are subjected to

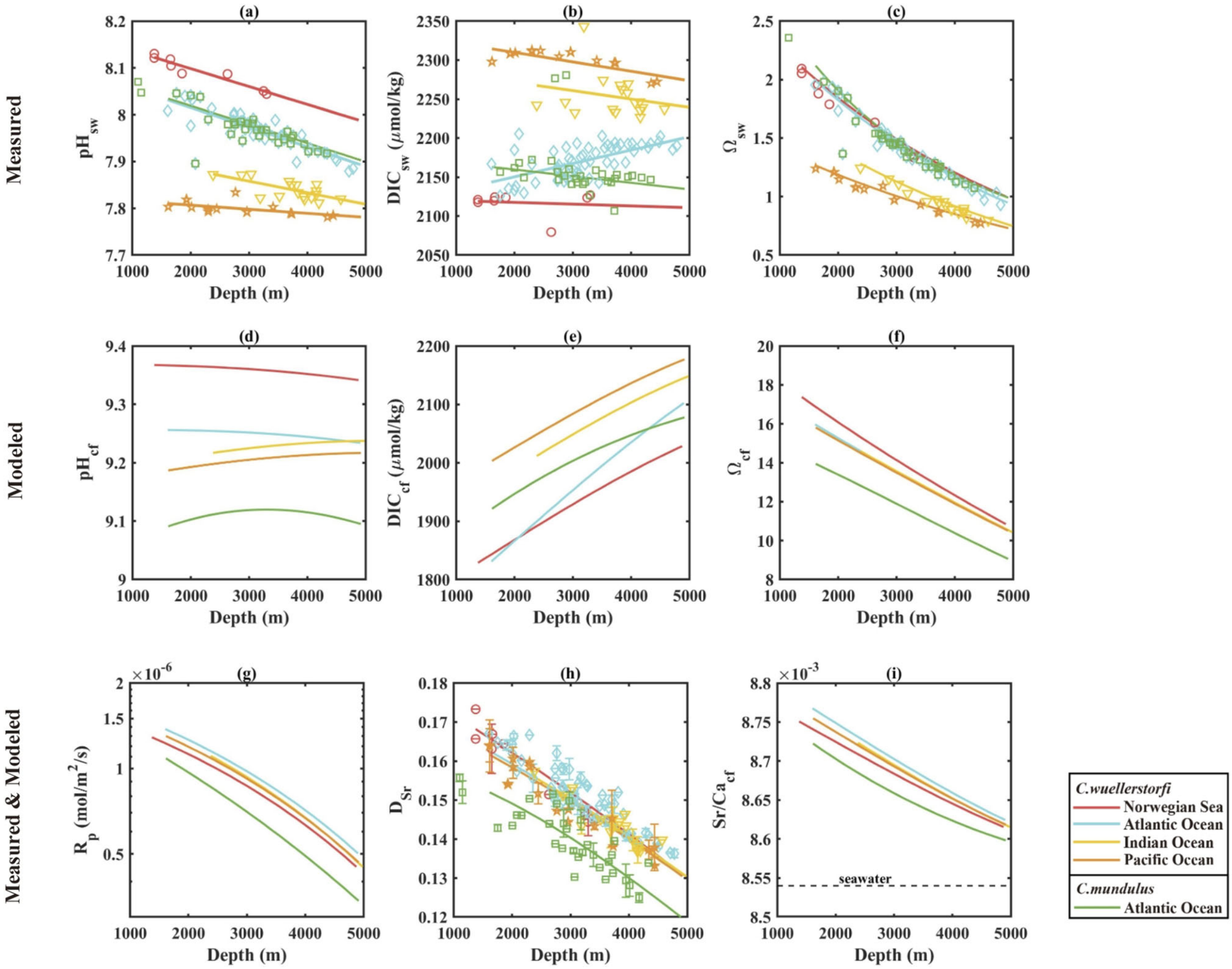

Fig. 3 Measured seawater chemistry and foraminiferal Sr partition coefficient (D_{Sr}), together with and modeled foraminiferal parameters. Measured and/or modeled (**a**) seawater pH, (**b**) seawater DIC, (**c**) calcite saturation state of seawater, (**d**) pH of the calcifying fluid, (**e**) DIC of the calcifying fluid, (**f**) calcite saturation state of the calcifying fluid, (**g**) calcite precipitation rate R_p, (**h**) foraminiferal Sr partition coefficient D_{Sr}, and (**i**) Sr/Ca ratio of the calcifying fluid at steady state. The data points are measured values[36] and the solid lines are model outputs at steady state. Red, blue, yellow and orange color represent *C. wuellerstorfi* in the Norwegian Sea, the Atlantic Ocean, the Indian Ocean and the Pacific Ocean, respectively. Green color represents *C.mundulus* in the Atlantic Ocean. Errors in (**h**) represent ±1σ of replicates.

the effects of alkalinity pumping (terms involving F_{ALK}), transmembrane ion transport (terms involving cell permeability P_{cell}), and carbonate precipitation (terms involving R_p). The only tunable parameters in our model are the cell permeability (P_{cell}) and efficiency of the proton pump (F_{ALK}) (see Method section) because we treat the parameters in the ion-by-ion model of inorganic calcite precipitation as known quantities. These include the kinetic (attachment/detachment frequencies) and thermodynamic parameters, which are calculated from previously characterized temperature and pressure conditions in the four oceans (Supplementary Table 1).

Known model inputs are the seawater temperature, pressure, pH, and DIC at different water depths of the Norwegian Sea, the Atlantic Ocean, the Indian Ocean and the Pacific Ocean (Fig. 3a–c). Both seawater pH and DIC change systematically with water depth in each of the four oceans and can thus be interpolated linearly with depth. The variation of seawater pH with depth is generally smaller than 0.1 unit, and the variation of seawater DIC with depth is about 50 μM[36]. Environmental Ω_{sw} mostly depends on water depth and varies from 2 at 1000 m, to <1 at 5000 m[36]. The depth-dependence of Ω_{sw} is caused by an increase in the calcite solubility product (K_{sp}) with increasing pressure. Outputs of the model are the steady state composition of the calcifying fluid (e.g., $\mathrm{pH_{cf}}$, $[\mathrm{DIC}]_{\mathrm{cf}}$, Ω_{cf}), calcite growth rate (R_p), and growth rate-dependent partitioning coefficient (D_{Sr}) in the foraminiferal calcite (Fig. 3d–i).

Foraminiferal calcification and Sr/Ca were also modeled using data from cultured studies[9,17,18]. For these, the model inputs are seawater temperature, pressure, pH and DIC as reported from the experimental studies. The experimental temperature ranges from 11.5 to 25.6 °C and pressure is 1 atmosphere. The variations of pH and DIC are larger than those in natural seawater, with pH varying between 7.5 to 8.6, and DIC varying between 1000 to 7000 μM (see Supplementary Notes 3).

Modeled chemistry of calcifying fluid and Sr partitioning in natural benthic foraminifera. We vary the parameters P_{cell} and F_{ALK} to match the measured D_{Sr} and then retrieve the steady state water composition of the calcifying fluid. There is a range of combinations of P_{cell} and F_{ALK} values that approach the measured D_{Sr} with different r^2 values, and we select the model parameters that result in the largest r^2 value (see Supplementary Notes 4). The model-inferred pH of 9.1–9.4 for the calcifying fluid is in good agreement with measurements from ref. [24], who reported

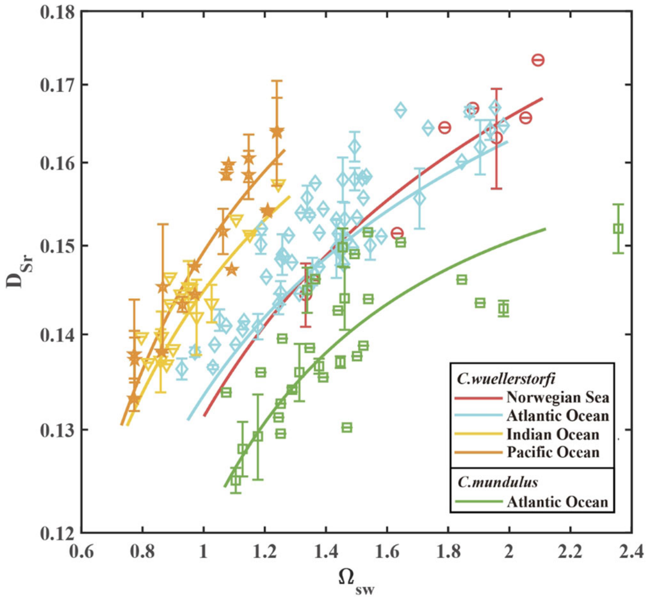

Fig. 4 Modeled and measured Sr partition coefficient between foraminifera calcite and environmental seawater (D_{Sr}) as a function of the seawater calcite saturation state (Ω_{sw}). The data points are measured values[36] and the solid lines are model outputs at steady state. Red, blue, yellow and orange color represent *C. wuellerstorfi* in the Norwegian Sea, the Atlantic Ocean, the Indian Ocean and the Pacific Ocean, respectively. Green color represents *C.mundulus* in the Atlantic Ocean. Error bars represent ±1σ of replicate analyses.

that foraminiferal calcite is precipitated in the hyaline species *Cibicides lobatulus* at pH >9.0, using the ratiometric fluorescent probe HPTS to visualize the intracellular pH.

Model outputs of R_p and D_{Sr} and associated carbonate chemistry in the calcifying fluid are plotted against the data in Fig. 3. The concentrations of individual DIC species are provided in Supplementary Notes 4, Fig. S5. A key result is that geographic and taxonomic differences in the foraminiferal D_{Sr} vs Ω_{sw} relationships are resolved by applying the same P_{cell} value (4×10^{-6} m/s) to both *C. wuellerstorfi* and *C. mundulus* but slightly different F_{ALK} values for *C. wuellerstorfi* (4.7×10^{-6} mol/m^2/s) and *C. mundulus* (3.9×10^{-6} mol/m^2/s). The modeled D_{Sr} versus Ω_{sw} (Fig. 4) indicate that although there are differences in Ω_{sw} in the four oceans, proton pumping by the foraminifera modifies the composition of the calcifying fluid leading to similar Ω_{cf} (and D_{Sr}) vs depth relationships for *C. wuellerstorfi* in the four oceans (Fig. 3f–h). The slightly lower F_{ALK} value for *C. mundulus* leads to lower Ω_{cf} and D_{Sr} for the same range of water depths.

In the model, the DIC in the calcifying fluid decreases by about 300 μM relative to environmental seawater due to calcite precipitation outpacing the DIC flux to the calcifying fluid. However, Ω_{cf} increases by about a factor of 10 due to the high pH_{cf}. The model precipitation rates of calcite range from 0.3 to 1.5×10^{-6} mol/m^2/s. We note that these are instantaneous rates, which are different from the average growth rates of foraminifera because the growth of foraminiferal calcite is episodic and intermittent[53]. Devriendt et al.[54] and Geerken et al.[55] independently estimated that the instantaneous rate of calcite precipitation for the low-Mg benthic foraminifera *Ammonia sp*. to be around 3.3 to 5.0×10^{-6} mol/m^2/s. This range is comparable to the inferred precipitation rate for *C. wuellerstorfi* and *C. mundulus* using our model. The higher inferred precipitation rate for *Ammonia sp*. relative to *C. wuellerstorfi* and *C. mundulus* could potentially be explained by a stronger alkalinity pump. In fact, a modeled precipitation rate of 4.6×10^{-6} mol/m^2/s (which is within the range obtained by Geerken et al.[55]) is attained when fitting the average D_{Sr} in Geerken et al.[55] at 25 °C and 1 atm with an identical P_{cell} value (4×10^{-6} m/s) but with F_{ALK} increased by a factor of 2 (8.0×10^{-6} mol/m^2/s).

Modeled Sr partitioning in culturing experiments. Culturing experiments of benthic[18] and planktonic[9,17] foraminifera provide more data on the influence of environmental changes on Sr partitioning in foraminifera beyond the modern natural variations of seawater pH and DIC. Supplementary Notes 3 provides a compilation of D_{Sr} data obtained from cultured foraminifera. There is a general increase in foraminiferal D_{Sr} with increasing seawater DIC, although differences in the D_{Sr} -DIC relationship exist between different cultured foraminifera species.

In our model for core top benthic foraminifera, the D_{Sr} data[36] can be fit using the same F_{ALK} and P_{cell} values for a given species across the range of seawater [DIC] and pH. In applying our model to benthic and planktonic foraminifera from culturing studies, we use the same P_{cell} value as applied to the field samples (4×10^{-6} m/s) and vary F_{ALK} until the model D_{Sr} matches the measured value (see Supplementary Notes 5 for an example calculation). Figure 5 shows the F_{ALK} values required to exactly fit the D_{Sr} data obtained from cultured foraminifera under more variable environmental conditions. Results indicate some inter-species variability in F_{ALK}, but for a given species F_{ALK} remains relatively constant across a broad range of external [DIC] and pH.

Implications for foraminiferal calcification, past and future. Assuming constant foraminiferal physiology through time, our model can be used to estimate how precipitation of foraminiferal calcite (R_p) may be affected by changes in atmospheric CO_2 concentration via the influence on seawater pH and DIC (Fig. 6a, b). Here, we apply constant P_{cell} (4×10^{-6} m/s) and F_{ALK} (5.8×10^{-6} mol/m^2/s, the average F_{ALK} of different planktic species[9,17]) values for our simulations to show how calcification and Sr partitioning of planktic foraminifera may have varied in the past or will vary in the future. The assumption of constant P_{cell} and F_{ALK} parameters in time is supported by a good data-model agreement when using a constant species-specific F_{ALK} value over a wide pH range (7.5–8.6; Fig. 5 and Supplementary Notes 5)[9,17].

The emission of anthropogenic CO_2 since the Industrial Revolution has led to ocean acidification with the average surface ocean pH decreasing from 8.2 (pre-industrialization) to 8.05 (in 2020)[56], DIC concentration increasing from 2000 to 2100 μmol/kg[57], and Ω decreasing from of 5.58 to 4.29. A 23% decrease in seawater Ω is associated with a 46% decrease (from 9.8×10^{-9} to 5.3×10^{-9} mol/m^2/s) in R_p for inorganic calcite[58] while our model indicates foraminiferal R_p would have decreased by about 2% (from 3.29×10^{-6} to 3.23×10^{-6} mol/m^2/s) in the upper part of the water column.

End of 21st century projections under the ‘business-as-usual’ scenario[56] imply an average surface ocean pH further decreasing to 7.73, DIC concentration increasing to 2360 μmol/kg, and Ω further decreasing to 2.39. These ocean conditions are associated with an 89% decrease in inorganic calcite precipitation rate[58] while the modeled foraminiferal R_p (~3.14×10^{-6} mol/m^2/s) decrease is only 5%.

These relatively small reductions in foraminiferal calcification rates in comparison to expected outcomes for inorganic calcite reflect homeostasis of the foraminiferal calcification fluid

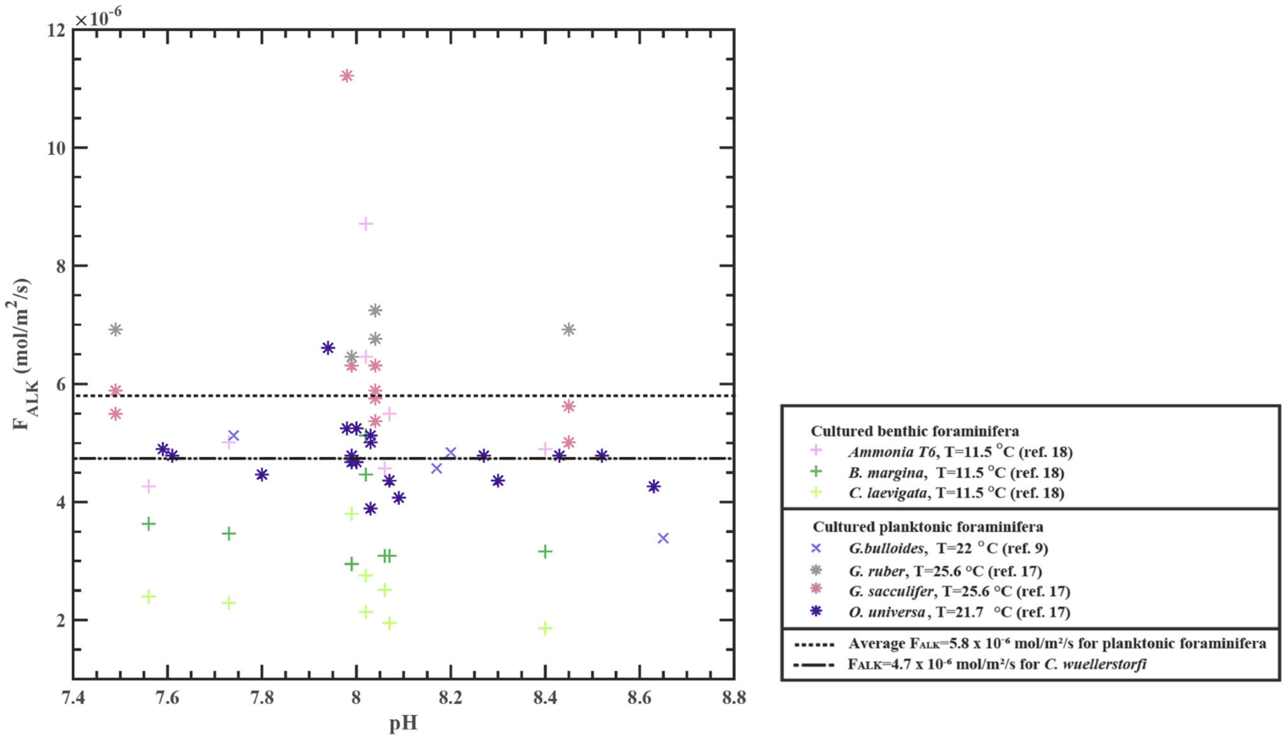

Fig. 5 Modeled alkalinity pump values (F_{ALK}) inferred from Sr partition coefficient (D_{Sr}) data obtained from cultured foraminifera under various environmental conditions. The cultured benthic foraminifera species are *Ammonia T6*[18] (pink cross), *B. margina*[18] (dark green cross) and C.laevigata[18] (light green cross). The cultured planktonic foraminifera species are *G. bulloides*[9] (purple cross), *G. ruber*[17] (gray asterisk), *G.sacculifer*[17] (pink asterisk), and *O.universa*[17] (purple asterisk). The cell permeability (P_{cell}) value for both benthic and planktonic foraminifera is 4×10^{-6} m/s. The dashed line represents the average proton pump rate (F_{ALK}) value (5.8×10^{-6} mol/m^2/s) across different planktonic species in changing environments. The dashdot line represents the F_{ALK} value (4.7×10^{-6} mol/m^2/s) to fit Sr partition coefficient (D_{Sr}) data of natural benthic foraminifera[36].

composition. This resilience of foraminifera calcification to ocean acidification is explained by the active proton pumping mechanism and by higher seawater DIC under increasing atmospheric CO_2 concentrations. This is because a higher DIC concentration in a foraminifer calcifying fluid leads to more HCO_3^- conversion to CO_3^{2-} when subject to the alkalinity pump. This compensates for the negative effect of a lower seawater pH on $[CO_3^{2-}]_{cf}$, and results in a near-constant Ω_{cf} and R_p.

Assuming the foraminiferal biomineralization model holds in the geological past, times of high atmospheric CO_2 (1000 ppmv) and surface ocean DIC (3900 µmol/kg) concentrations in the late Eocene[59] (ca. 35 Ma) may have favored foraminiferal calcification as our model indicates R_p values would have increased to 3.98×10^{-6} mol/m^2/s, up by some 21% compared to the recent pre-industrial time. This supports evidence for the large planktonic foraminiferal test size and high number of species during the Late Eocene[60].

The model may also be used to estimate foraminiferal D_{Sr} values and seawater Sr/Ca throughout geological history. For example, Lear et al.[35] calibrated D_{Sr} values using modern benthic foraminifera against water depth for different foraminifera species. They then calculated the Cenozoic seawater Sr/Ca ratio using measured foraminiferal Sr/Ca with calibrated D_{Sr} values. However, in the early and middle Cenozoic, the seawater temperature was higher and seawater pH was lower, possibly leading to lower D_{Sr} than the calibrations based on modern foraminifera would indicate[61]. Taking these temperature and pH effects into account, the modeled D_{Sr} value of foraminifera that calcified 50 Ma ago (pH = 7.5, DIC = 2200 µmol/kg, surface seawater temperature = 35.2 °C[62]) is 0.122 which is 24% lower than the modeled D_{Sr} value of modern foraminifera (0.160) that live in surface seawater with pH of about 8.1, DIC of about 2100 µmol/kg and temperature of about 18 °C[57,63] (Fig. 6c). It is worth noting that within the 24% decrease in D_{Sr} only 2.5% is due to the lower pH and higher DIC at 50 Ma and the rest of the decrease in D_{Sr} is due to the higher temperature (Fig. 6c). As a result, previous work[35] may have underestimated seawater Sr/Ca in the Cenozoic by assuming a Sr partitioning coefficient that is only depth- and species-dependent. Assuming an average Sr/Ca ratio of 2.3 mM/M in rock weathering inputs to oceans, a partition coefficient of 0.15 for calcite and 1.0 for aragonite, and seawater Sr/Ca ratio around 8 mM/M at 50 Ma[64], an underestimated seawater Sr/Ca by 24% leads to an underestimation of the fraction of oceanic Ca removal by calcite by about 8% (0.83 compared to 0.90).

Several caveats require attention in the above calculations. First, our model is a simplified description of the calcification process. Additional processes are thought to occur in foraminifera that affect trace element partitioning and isotope fractionation, such as cross membrane transport of ions that may be discriminating against certain elements[25] and precipitation of metastable amorphous calcium carbonate[65] and/or vaterite and their recrystallization to calcite[66]. Our model does not invoke precursor phases, but relies on the elevation of pH in the calcifying fluid (and exclusion of Mg^{2+}) and Sr/Ca partitioning information from inorganic calcite to explain the observed D_{Sr} data. Second, an adaption of foraminifera calcification strategies through geological history and possibly in the future is possible and was not considered in the calculation above. Variable F_{ALK} and P_{cell} values in deep time and in the future cannot be excluded, although our result indicates that Sr uptake by foraminifers under a wide range of

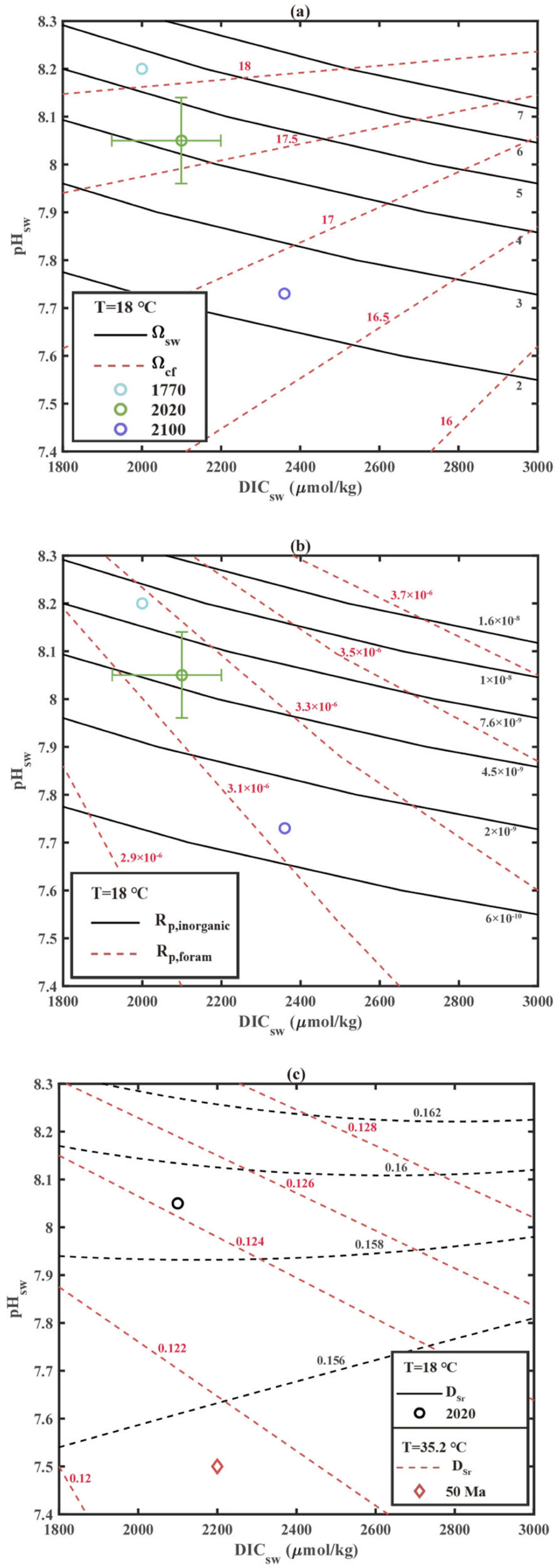

Fig. 6 Effects of seawater DIC (DIC_{sw}) and pH (pH_{sw}) on foraminiferal and inorganic calcite precipitation, and foraminiferal Sr partitioning near the surface (T = 18 °C or 35.2 °C, pressure = 1 atm). Blue, green and purple circles represent the seawater chemistry in 1770, 2020 and 2100, respectively. Bars on the 2020 circle represent spatial and seasonal variability in pH_{sw} (7.96–8.16) and DIC_{sw} (1900–2200 μmol/kg)[56]. **a** Calcite saturation state of seawater (Ω_{sw}: black solid lines) and the calcifying fluid of *C. wuellerstorfi* (Ω_{cf}: red dashed lines) as a function of DIC_{sw} and pH_{sw}. **b** Calcite growth rate (R_p in mol/m^2/s) for inorganic calcite (black solid lines) and foraminiferal calcite (red dashed lines) as a function of DIC_{sw} and pH_{sw}. Values of inorganic calcite R_p are calculated as a function of temperature and Ω[58]. **c** Foraminiferal Sr partition coefficient (D_{Sr}) at 35.2 °C[62] (red dashed lines) and 18 °C (black dashed lines) as a function of DIC_{sw} and pH_{sw}.

environmental conditions is well predicted without a change in foraminifer physiology. In Supplementary Notes 6, we show the effects of F_{ALK} on foraminiferal D_{Sr} and R_p and the uncertainty in F_{ALK} (represented by one standard deviation of F_{ALK} values of individual species derived from Fig. 5). Our conclusion that D_{Sr} is lower during Cenozoic is largely independent of uncertainties in F_{ALK} but predictions of R_p may be more uncertain. Overall, the results presented here highlight the expected trends on future and past calcification and Sr partitioning in foraminifera based on our current understanding of biomineralization processes.

Conclusion

The model presented here takes seawater chemistry, temperature, and pressure as inputs, and calculates the concentration of carbonate species in the calcifying fluid, the precipitation rate of calcite, and the foraminiferal D_{Sr} value. The tunable parameters are the alkalinity pump rate (F_{ALK}) and the cell permeability coefficient (P_{cell}). The good agreement between model results and core-top data from various ocean basins demonstrates that D_{Sr} values in benthic foraminifera can be explained by inorganic-like partitioning within a biologically-modified calcifying fluid. Furthermore, applying our model to culturing experiments suggests that for a given foraminifera species, the alkalinity pumping rate remains relatively stable across a broad range of DIC and pH levels. The proton pump in foraminifera leads to a homeostasis of the calcifying fluid, which could explain why foraminifera have been resilient to changes in ocean carbonate chemistry over geological timescales. Nevertheless, our model indicates that foraminiferal D_{Sr} values were likely lower than their modern values during the early and middle Cenozoic due to overall higher seawater temperature.

Method

Samples. Sr/Ca data of two calcitic benthic foraminiferal species (*C. wuellerstorfi* and *C. mundulus*) from the global oceans were analysed by ref. [36]. To minimize the influence of shell size[32], each measurement contains 10–15 shells from the 250–500 μm size fraction. Duplicate analyses (213 Sr/Ca measurements for 136 core tops) were made and the uncertainty of measured Sr/Ca data is about ±1% (1σ). The data we use are the average of duplicate measurements.

Model structure. We consider five processes during the calcification of foraminiferal calcite: seawater leak, ion transport by diffusion, active proton pumping (or alkalinity pump), CO_2 diffusion and calcite precipitation. The site of calcification is conceptualized as a box with unit surface area and a height of z (in μm). Sr^{2+}, Ca^{2+}, HCO_3^-, CO_3^{2-}, OH^- and H^+ enter the site of calcification through transmembrane transport with rates that are proportional to their concentration difference inside and outside the site of calcification[25,67]. A membrane permeability coefficient is assigned to all the ion chemical species (P_{cell}, in m/s).

Following Chen et al.[28], the differential equations for the chemical components in the calcifying fluid (DIC, ALK, $[Ca^{2+}]$, and $[Sr^{2+}]$) are:

$$\frac{d[\mathrm{DIC}]}{dt} = \frac{1}{\tau_{sw}}\left([\mathrm{DIC}]_{sw} - [\mathrm{DIC}]\right) + \frac{P_{HCO_3^-}}{z}\left(\left[\mathrm{HCO_3^-}\right]_{sw} - \left[\mathrm{HCO_3^-}\right]\right) + \frac{P_{CO_3^{2-}}}{z}\left(\left[\mathrm{CO_3^{2-}}\right]_{sw} - \left[\mathrm{CO_3^{2-}}\right]\right) + \frac{D_{CO_2}}{z}\left(\left[\mathrm{CO_2}\right]_{cell} - \left[\mathrm{CO_2}\right]\right) - \frac{R_p}{1000z} \tag{2a}$$

$$\frac{d[\mathrm{ALK}]}{dt} = \frac{1}{\tau_{sw}}\left([\mathrm{ALK}]_{sw} - [\mathrm{ALK}]\right) + \frac{P_{HCO_3^-}}{z}\left(\left[\mathrm{HCO_3^-}\right]_{sw} - \left[\mathrm{HCO_3^-}\right]\right) + 2\frac{P_{CO_3^{2-}}}{z}\left(\left[\mathrm{CO_3^{2-}}\right]_{sw} - \left[\mathrm{CO_3^{2-}}\right]\right) + \frac{1}{1000z}\left(F_{ALK} - 2R_p\right) + \frac{P_{OH^-}}{z}\left([OH^-]_{sw} - [OH^-]\right) - \frac{P_{H^+}}{z}\left(\left[H^+\right]_{sw} - \left[H^+\right]\right) \tag{2b}$$

$$\frac{d\left[\mathrm{Ca^{2+}}\right]}{dt} = \frac{1}{\tau_{sw}}\left(\left[\mathrm{Ca^{2+}}\right]_{sw} - \left[\mathrm{Ca^{2+}}\right]\right) + \frac{P_{Ca^{2+}}}{z}\left(\left[\mathrm{Ca^{2+}}\right]_{sw} - \left[\mathrm{Ca^{2+}}\right]\right) - \frac{R_p}{1000z}\left(1 - x_c\right) + \frac{F_{ALK}}{1000 \cdot 2z} f\left(1 - x_{sw}\right) \tag{2c}$$

$$\frac{d\left[\mathrm{Sr^{2+}}\right]}{dt} = \frac{1}{\tau_{sw}}\left(\left[\mathrm{Sr^{2+}}\right]_{sw} - \left[\mathrm{Sr^{2+}}\right]\right) + \frac{P_{Sr^{2+}}}{z}\left(\left[\mathrm{Sr^{2+}}\right]_{sw} - \left[\mathrm{Sr^{2+}}\right]\right) - \frac{R_p}{1000z} x_c + \frac{F_{ALK}}{1000 \cdot 2z} f x_{sw} \tag{2d}$$

where τ_{sw} (s) is seawater residence time in the calcifying fluid, R_p (mol/m^2/s) is calcite precipitation rate, F_{ALK} (mol/m^2/s) is proton pump rate, x_c is the Sr fraction in calcite ($x_c = [Sr]_c/([Sr]_c + [Ca]_c)$), z (μm) is the thickness of the calcifying fluid, D_{CO_2} (m/s) is cell permeability of CO_2, f is fraction of Sr^{2+} and Ca^{2+} in exchange of H^+, $[CO_2]_{cell}$ (mol/L) is cell CO_2 concentration, x_{sw} is the Sr^{2+} fraction in seawater ($x_{sw} = [Sr]_{sw}/([Sr]_{sw} + [Ca]_{sw})$) and the *sw* subscript denotes the concentration of a chemical component in seawater. In our default model the seawater leakage terms (term with τ_{sw}) are set to zero because the data we fit are all from low-Mg calcite, where transmembrane transport is the primary mechanism through which foraminifera gains ions for calcification (see Supplementary Notes 2).

The model solves for [DIC], [ALK], $[Ca^{2+}]$ and $[Sr^{2+}]$ in the calcifying fluid. Their initial values are set equal to those in seawater, and Eqs. (2a–d) are solved until a steady state is reached, i.e., when the time derivative terms on the left of the equations are equal to zero. The final results are steady state values of $[\mathrm{DIC}]_{cf}$, $[\mathrm{ALK}]_{cf}$, $[Ca^{2+}]_{cf}$, and $[Sr^{2+}]_{cf}$, from which the steady state calcite precipitation rate and D_{Sr} can be retrieved by extended ion-by-ion model for Sr partitioning[8] (see Supplementary Notes 7). Our model assumes that the speciation of DIC is instantaneous so that with the modeled DIC and ALK values in Eqs. (2a, b) it is possible to calculate the full carbonate chemistry of the fluid. This assumption is supported by the fact that the chemical equilibration time for DIC species is on the order of seconds[57] and the presence of enzyme carbonic anhydrase in foraminifera further shorten the equilibration time[49].

Data availability

Sample data associated with this article can be accessed at the Github repository https://github.com/shuozhangthu/Dsr_foram.

Code availability

All analysis was conducted in MATLAB R2020b. Model code associated with this article can be accessed at the Github repository https://github.com/shuozhangthu/Dsr_foram.

Received: 10 April 2023; Accepted: 21 December 2023;
Published online: 12 January 2024

References

1. Lorens, R. B. Sr, Cd, Mn and Co distribution coefficients in calcite as a function of calcite precipitation rate. *Geochim. Cosmochim. Acta* **45**, 553–561 (1981).
2. Tesoriero, A. J. & Pankow, J. F. Solid solution partitioning of Sr^{2+}, Ba^{2+}, and Cd^{2+} to calcite. *Geochim. Cosmochim. Acta* **60**, 1053–1063 (1996).
3. Tang, J., Köhler, S. J. & Dietzel, M. Sr^{2+}/Ca^{2+} and $^{44}Ca/^{40}Ca$ fractionation during inorganic calcite formation: I. Sr incorporation. *Geochim. Cosmochim. Acta* **72**, 3718–3732 (2008).
4. Morse, J. W. & Bender, M. L. Partition coefficients in calcite: examination of factors influencing the validity of experimental results and their application to natural systems. *Chem. Geol* **82**, 265–277 (1990).
5. Katz, A., Sass, E. & Starinsky, A. Strontium behavior in the aragonite–calcite transformation: an experimental study at 40–98°C. *Geochim. Cosmochim. Acta* **36**, 481–496 (1972).
6. Pingitore, N. E. Jr. & Eastman, M. P. The coprecipitation of Sr^{2+} with calcite at 25 °C and 1 atm. *Geochim. Cosmochim. Acta* **50**, 2195–2203 (1986).
7. Zhang, S. & DePaolo, D. J. Equilibrium calcite-fluid Sr/Ca partition coefficient from marine sediment and pore fluids. *Geochim. Cosmochim. Acta* **289**, 33–46 (2020).
8. Jia, Q., Zhang, S., Lammers, L., Huang, Y. & Wang, G. A model for pH dependent strontium partitioning during calcite precipitation from aqueous solutions. *Chem. Geol.* **608**, https://doi.org/10.1016/j.chemgeo.2022.121042 (2022).
9. Russell, A. D., Hönisch, B., Spero, H. J. & Lea, D. W. Effects of seawater carbonate ion concentration and temperature on shell U, Mg, and Sr in cultured planktonic foraminifera. *Geochim. Cosmochim. Acta* **68**, 4347–4361 (2004).
10. Dueñas-Bohórquez, A., da Rocha, R. E., Kuroyanagi, A., Bijma, J. & Reichart, G.-J. Effect of salinity and seawater calcite saturation state on Mg and Sr incorporation in cultured planktonic foraminifera. *Mar. Micropaleontol.* **73**, 178–189 (2009).
11. Raitzsch, M., Duenas-Bohorquez, A., Reichart, G. J., de Nooijer, L. J. & Bickert, T. Incorporation of Mg and Sr in calcite of cultured benthic foraminifera: impact of calcium concentration and associated calcite saturation state. *Biogeosciences* **7**, 869–881 (2010).
12. Dissard, D., Nehrke, G., Reichart, G.-J. & Bijma, J. Impact of seawater pCO_2 on calcification and Mg/Ca and Sr/Ca ratios in benthic foraminifera calcite: results from culturing experiments with *Ammonia tepida*. *Biogeosciences* **7**, 81–93 (2010).
13. Dueñas-Bohórquez, A., Raitzsch, M., de Nooijer, L. J. & Reichart, G.-J. Independent impacts of calcium and carbonate ion concentration on Mg and Sr incorporation in cultured benthic foraminifera. *Mar. Micropaleontol.* **81**, 122–130 (2011).
14. Keul, N. et al. Exploring foraminiferal Sr/Ca as a new carbonate system proxy. *Geochim. Cosmochim. Acta* **202**, 374–386 (2017).
15. Not, C., Thibodeau, B. & Yokoyama, Y. Incorporation of Mg, Sr, Ba, U, and B in high-Mg calcite benthic foraminifers cultured under controlled pCO_2. *Geochem. Geophys. Geosyst.* **19**, 83–98 (2018).
16. Kısakürek, B., Eisenhauer, A., Böhm, F., Hathorne, E. C. & Erez, J. Controls on calcium isotope fractionation in cultured planktic foraminifera, *Globigerinoides ruber* and *Globigerinella siphonifera*. *Geochim. Cosmochim. Acta* **75**, 427–443 (2011).
17. Allen, K. A. et al. Trace element proxies for surface ocean conditions: a synthesis of culture calibrations with planktic foraminifera. *Geochim. Cosmochim. Acta* **193**, 197–221 (2016).

18. Mojtahid, M. et al. Assessing the impact of different carbonate system parameters on benthic foraminifera from controlled growth experiments. *Chem. Geol*. **623**, https://doi.org/10.1016/j.chemgeo.2023.121396 (2023).
19. Duplessy, J. C., Lalou, C. & Vinot, A. C. Differential isotopic fractionation in benthic foraminifera and paleotemperatures reassessed. *Science* **168**, 250–251 (1970).
20. McConnaughey, T. ^{13}C and ^{18}O isotopic disequilibrium in biological carbonates: I. Patterns. *Geochim. Cosmochim. Acta* **53**, 151–162 (1989).
21. de Villiers, S., Nelson, B. K. & Chivas, A. R. Biological controls on Coral Sr/Ca and $\delta^{18}O$ reconstructions of sea surface temperatures. *Science* **269**, 1247–1249 (1995).
22. Stephenson, A. E. et al. Peptides enhance magnesium signature in calcite: insights into origins of vital effects. *Science* **322**, 724–727 (2008).
23. Bentov, S., Brownlee, C. & Erez, J. The role of seawater endocytosis in the biominer alization process in calcareous foraminifera. *PNAS* **106**, 21500–21504 (2009).
24. de Nooijer, L., Toyofuku, T. & Kitazato, H. Foraminifera promote calcification by elevating their intracellular pH. *PNAS* **106**, 15374–15378 (2009).
25. de Nooijer, L. J., Spero, H. J., Erez, J., Bijma, J. & Reichart, G. J. Biomineralization in perforate foraminifera. *Earth-Science Reviews* **135**, 48–58 (2014).
26. Erez, J. The source of ions for biomineralization in foraminifera and their implications for paleoceanographic proxies. *Rev. Mineral. Geochem.* **54**, 115–149 (2003).
27. Bentov, S. & Erez, J. Impact of biomineralization processes on the Mg content of foraminiferal shells: a biological perspective. *Geochem. Geophys. Geosyst.* **7**, https://doi.org/10.1029/2005gc001015 (2006).
28. Chen, S., Gagnon, A. C. & Adkins, J. F. Carbonic anhydrase, coral calcification and a new model of stable isotope vital effects. *Geochim. Cosmochim. Acta* **236**, 179–197 (2018).
29. Elderfield, H., Cooper, M. & Ganssen, G. Sr/Ca in multiple species of planktonic foraminifera: Implications for reconstructions of seawater Sr/Ca. *Geochem. Geophys. Geosyst*. **1**, https://doi.org/10.1029/1999gc000031 (2000).
30. Dissard, D. et al. Mg/Ca, Sr/Ca and stable isotopes from the planktonic foraminifera *T. sacculifer*: testing a multi-proxy approach for inferring paleotemperature and paleosalinity. *Biogeosciences* **18**, 423–439 (2021).
31. Cléroux, C. et al. Mg/Ca and Sr/Ca ratios in planktonic foraminifera: Proxies for upper water column temperature reconstruction. *Paleoceanography* **23**, https://doi.org/10.1029/2007pa001505 (2008).
32. Elderfield, H., Vautravers, M., Cooper, M. The relationship between shell size and Mg/Ca, Sr/Ca, $\delta^{18}O$, and $\delta^{13}C$ of species of planktonic foraminifera. *Geochem. Geophys. Geosyst*. **3**, https://doi.org/10.1029/2001GC000194 (2002).
33. Rosenthal, Y. et al. Interlaboratory comparison study of Mg/Ca and Sr/Ca measurements in planktonic foraminifera for paleoceanographic research. *Geochem. Geophys. Geosyst*. **5**, https://doi.org/10.1029/2003gc000650 (2004).
34. Anand, P. & Elderfield, H. Variability of Mg/Ca and Sr/Ca between and within the planktonic foraminifers *Globigerina bulloides* and *Globorotalia truncatulinoides*. *Geochem. Geophys. Geosyst*. **6**, https://doi.org/10.1029/2004gc000811 (2005).
35. Lear, C. H., Elderfield, H. & Wilson, P. A. A Cenozoic seawater Sr/Ca record from benthic foraminiferal calcite and its application in determining global weathering fluxes. *Earth Planet. Sci. Lett.* **208**, 69–84 (2003).
36. Yu, J. M., Elderfield, H., Jin, Z. D., Tomascak, P. & Rohling, E. J. Controls on Sr/Ca in benthic foraminifera and implications for seawater Sr/Ca during the late Pleistocene. *Quaternary Sci. Rev*. **98**, 1–6 (2014).
37. Rathburn, A. E. & DeDeckker, P. Magnesium and strontium compositions of Recent benthic foraminifera from the Coral Sea, Australia and Prydz Bay, Antarctica. *Mar. Micropaleontol.* **32**, 231–248 (1997).
38. Martin, P. A., Lea, D. W., Mashiotta, T. A., Papenfuss, T. & Sarnthein, M. Variation of foraminiferal Sr/Ca over Quaternary glacial-interglacial cycles: evidence for changes in mean ocean Sr/Ca? *Geochem. Geophys. Geosyst*. **1**, https://doi.org/10.1029/1999gc000006 (2000).
39. Rosenthal, Y., Lear, C. H., Oppo, D. W. & Linsley, B. K. Temperature and carbonate ion effects on Mg/Ca and Sr/Ca ratios in benthic foraminifera: Aragonitic species *Hoeglundina elegans*. *Paleoceanography* **21**, https://doi.org/10.1029/2005pa001158 (2006).
40. Dawber, C. F. & Tripati, A. K. Exploring the controls on element ratios in middle Eocene samples of the benthic foraminifera *Oridorsalis umbonatus*. *Clim. Past* **8**, 1957–1971 (2012).
41. Raja, R., Saraswati, P. K. & Iwao, K. A field-based study on variation in Mg/Ca and Sr/Ca in larger benthic foraminifera. *Geochem. Geophys. Geosyst*. **8**, https://doi.org/10.1029/2006gc001478 (2007).
42. Rathmann, S. & Kuhnert, H. Carbonate ion effect on Mg/Ca, Sr/Ca and stable isotopes on the benthic foraminifera *Oridorsalis umbonatus* off Namibia. *Mar. Micropaleontol.* **66**, 120–133 (2008).
43. Dawber, C. F. & Tripati, A. Relationships between bottom water carbonate saturation and element/Ca ratios in coretop samples of the benthic foraminifera *Oridorsalis umbonatus*. *Biogeosciences* **9**, 3029–3045 (2012).
44. Yu, Z., Lei, Y., Li, T., Zhang, S. & Xiong, Z. Mg and Sr uptake in benthic foraminifera *Ammonia aomoriensis* based on culture and field studies. *Palaeogeogr. Palaeoclimatol. Palaeoecol.* **520**, 229–239 (2019).
45. Key, R. M. et al. A global ocean carbon climatology: Results from Global Data Analysis Project (GLODAP). *Global Biogeochem. Cycles* **18**, https://doi.org/10.1029/2004gb002247 (2004).
46. Mucci, A. & Morse, J. W. The incorporation of Mg^{2+} and Sr^{2+} into calcite overgrowths: influences of growth rate and solution composition. *Geochim. Cosmochim. Acta* **47**, 217–233 (1983).
47. Nehrke, G. et al. A new model for biomineralization and trace-element signatures of Foraminifera tests. *Biogeosciences* **10**, 6759–6767 (2013).
48. Toyofuku, T. et al. Proton pumping accompanies calcification in foraminifera. *Nat. Commun.* **8**, 14145 (2017).
49. de Goeyse, S., Webb, A. E., Reichart, G.-J. & de Nooijer, L. J. Carbonic anhydrase is involved in calcification by the benthic foraminifer *Amphistegina lessonii*. *Biogeosciences* **18**, 393–401 (2021).
50. Zeebe, R. E. An explanation of the effect of seawater carbonate concentration on foraminiferal oxygen isotopes. *Geochim. Cosmochim. Acta* **63**, 2001–2007 (1999).
51. Devriendt, L. S., McGregor, H. V. & Chivas, A. R. Ostracod calcite records the $^{18}O/^{16}O$ ratio of the bicarbonate and carbonate ions in water. *Geochim. Cosmochim. Acta* **214**, 30–50 (2017).
52. Devriendt, L. S., Watkins, J. M. & McGregor, H. V. Oxygen isotope fractionation in the $CaCO_3$-DIC-H_2O system. *Geochim. Cosmochim. Acta* **214**, 115–142 (2017).
53. Farmer, J. R. et al. Boric acid and borate incorporation in inorganic calcite inferred from B/Ca, boron isotopes and surface kinetic modeling. *Geochim. Cosmochim. Acta* **244**, 229–247 (2019).
54. Devriendt, L. S. et al. Sodium incorporation into inorganic $CaCO_3$ and implications for biogenic carbonates. *Geochim. Cosmochim. Acta* **314**, 294–312 (2021).
55. Geerken, E. et al. High precipitation rates characterize biomineralization in the benthic foraminifer *Ammonia beccarii*. *Geochim. Cosmochim. Acta* **318**, 70–82 (2022).
56. Jiang, L. Q., Carter, B. R., Feely, R. A., Lauvset, S. K. & Olsen, A. Surface ocean pH and buffer capacity: past, present and future. *Sci Rep* **9**, 18624 (2019).
57. Zeebe, R. E. & Wolf-Gladrow, D. A. CO_2 in Seawater, Equilibrium, Kinetics, Isotopes. vol. 65, 1–346. (Amsterdam - Boston – London - New York - Oxford - Paris - San Diego - San Francisco - Singapore - Sydney, Elsevier Science Limited, 2001).
58. Lopez, O., Zuddas, P. & Faivre, D. The influence of temperature and seawater composition on calcite crystal growth mechanisms and kinetics: Implications for Mg incorporation in calcite lattice. *Geochim. Cosmochim. Acta* **73**, 337–347 (2009).
59. Rae, J. W. B. et al. Atmospheric CO_2 over the past 66 million years from marine archives. *Annu. Rev. Earth Planet Sci.* **49**, 609–641 (2021).
60. Schmidt, D. N., Thierstein, H. R., Bollmann, J. & Schiebel, R. Abiotic forcing of plankton evolution in the Cenozoic. *Science* **303**, 207–210 (2004).
61. Turchyn, A. V. & DePaolo, D. J. Seawater chemistry through Phanerozoic time. *Annu. Rev. Earth Planet Sci.* **47**, 197–224 (2019).
62. Anagnostou, E. et al. Proxy evidence for state-dependence of climate sensitivity in the Eocene greenhouse. *Nat. Commun.* **11**, 4436 (2020).
63. Bopp, L. et al. Multiple stressors of ocean ecosystems in the 21st century: projections with CMIP5 models. *Biogeosciences* **10**, 6225–6245 (2013).
64. Zhang, S., Zhou, R. J. & DePaolo, D. J. The seawater Sr/Ca ratio in the past 50 Myr from bulk carbonate sediments corrected for diagenesis. *Earth Planet. Sci. Lett.* **530**, 115949 (2020).
65. Gilbert, P. U. P. A. & Wilt, F. H. in *Molecular Biomineralization: Aquatic Organisms Forming Extraordinary Materials* (ed Müller, W. E. G.) 199–223 (Springer, 2011).
66. Jacob, D. E., Wirth, R., Agbaje, O. B. A., Branson, O. & Eggins, S. M. Planktic foraminifera form their shells via metastable carbonate phases. *Nat. Commun.* **8**, 1265 (2017).
67. Higgins, C. F. ABC transporters: from microorganisms to man. *Annu. Rev. Cell Bio.l* **8**, 67–113 (1992).
68. Watkins, J. M. & Devriendt, L. S. A combined model for kinetic clumped isotope effects in the CaCO3-DIC-H2O system. *Geochem. Geophys. Geosyst.* **23**, e2021GC010200 (2022).

Acknowledgements

The structure of the box model code comes from Watkins and Devriendt (2022)[68]. S.Z. is funded by a startup fund from Tsinghua University. J.M.W. was supported by the National Science Foundation under NSF-CAREER Grant No. EAR1749183. We thank four anonymous reviewers for insightful comments.

Author contributions

Q.J. and S.Z. developed the model. Q.J., S.Z., J.M.W., and L.S.D. interpreted the results. Q.J., S.Z., J.M.W., L.S.D., Y.H., and G.W. wrote and revised the manuscript.

Competing interests
The authors declare no competing interests.

Additional information
Supplementary information The online version contains supplementary material available at https://doi.org/10.1038/s43247-023-01194-6.

Correspondence and requests for materials should be addressed to Shuo Zhang.

Peer review information *Communications Earth and Environment* thanks Takashi Toyofuku and the other, anonymous, reviewer(s) for their contribution to the peer review of this work. Primary Handling Editors: Yama Dixit and Clare Davis. A peer review file is available.